Publication Year	2024
Acceptance in OA	2025-04-14T11:53:46Z
Title	JOYS: Disentangling the warm and cold material in the high-mass IRAS 23385+6053 cluster (Corrigendum DOI: 10.1051/0004-6361/202347060)
Authors	Gieser, C., Beuther, H., van Dishoeck, E. F., Francis, L., van Gelder, M. L., Tychoniec, L., Kavanagh, P. J., Perotti, G., CARATTI O GARATTI, Alessio, Ray, T. P., Klaassen, P., Justtanont, K., Linnartz, H., Rocha, W. R. M., Slavicinska, K., Colina, L., Güdel, M., Henning, Th., Lagage, P.-O., Östlin, G., Vandenbussche, B., Waelkens, C., Wright, G.
Publisher's version (DOI)	10.1051/0004-6361/202450520e
Handle	http://hdl.handle.net/20.500.12386/37063
Journal	ASTRONOMY & ASTROPHYSICS
Volume	685

A&A, 685, C5 (2024)
https://doi.org/10.1051/0004-6361/202450520e

Astronomy & Astrophysics

JOYS: Disentangling the warm and cold material in the high-mass IRAS 23385+6053 cluster (*Corrigendum*)

C. Gieser[1,2], H. Beuther[2], E. F. van Dishoeck[3,1], L. Francis[3], M. L. van Gelder[3], L. Tychoniec[4], P. J. Kavanagh[5], G. Perotti[2], A. Caratti o Garatti[6], T. P. Ray[7], P. Klaassen[8], K. Justtanont[9], H. Linnartz[10], W. R. M. Rocha[3,10], K. Slavicinska[3,10], L. Colina[11], M. Güdel[12,2,13], Th. Henning[2], P.-O. Lagage[14], G. Östlin[15], B. Vandenbussche[16], C. Waelkens[16], and G. Wright[8]

[1] Max Planck Institute for Extraterrestrial Physics, Gießenbachstraße 1, 85749 Garching bei München, Germany
e-mail: gieser@mpe.mpg.de
[2] Max Planck Institute for Astronomy, Königstuhl 17, 69117 Heidelberg, Germany
[3] Leiden Observatory, Leiden University, PO Box 9513, 2300 RA Leiden, The Netherlands
[4] European Southern Observatory, Karl-Schwarzschild-Strasse 2, 85748 Garching bei München, Germany
[5] Department of Experimental Physics, Maynooth University-National University of Ireland Maynooth, Maynooth, Co Kildare, Ireland
[6] INAF-Osservatorio Astronomico di Capodimonte, Salita Moiariello 16, 80131 Napoli, Italy
[7] Dublin Institute for Advanced Studies, 31 Fitzwilliam Place, Dublin D02 XF86, Ireland
[8] UK Astronomy Technology Centre, Royal Observatory Edinburgh, Blackford Hill, Edinburgh EH9 3HJ, UK
[9] Department of Space, Earth and Environment, Chalmers University of Technology, Onsala Space Observatory, 439 92 Onsala, Sweden
[10] Laboratory for Astrophysics, Leiden Observatory, Leiden University, PO Box 9513, NL 2300 RA Leiden, The Netherlands
[11] Centro de Astrobiologıa (CAB, CSIC-INTA), Carretera de Ajalvir, 8850 Torrejon de Ardoz, Madrid, Spain
[12] Department of Astrophysics, University of Vienna, Türkenschanzstr. 17, 1180 Vienna, Austria
[13] ETH Zürich, Institute for Particle Physics and Astrophysics, Wolfgang-Pauli-Str. 27, 8093 Zürich, Switzerland
[14] Université Paris-Saclay, Université de Paris, CEA, CNRS, AIM, 91191 Gif-sur-Yvette, France
[15] Department of Astronomy, Oskar Klein Centre, Stockholm University, 106 91 Stockholm, Sweden
[16] Instituut voor Sterrenkunde, KU Leuven, Celestijnenlaan 200D, Bus-2410, 3000 Leuven, Belgium

A&A, 679, A108 (2023), https://doi.org/10.1051/0004-6361/202347060

Key words. stars: formation – ISM: individual objects: IRAS 23385+6053 – stars: jets – stars: massive – errata, addenda

1. Introduction

In the original article (Gieser et al. 2023), in Sect. 3.3 an error occurred in the code of the calculation of the H_2 line-integrated intensities estimated from a Gaussian fit. Due to this mistake, we overestimated the H_2 line-integrated intensities by a factor of $(\lambda[\mu\mathrm{m}])^2$. The observed line-integrated intensities were used to estimate the H_2 temperature and column density, with a warm and hot component. While the conclusions of the study remain qualitatively unchanged, here we provide correct values for the line-integrated intensities as well as for the H_2 temperatures and column densities.

The corrected H_2 excitation diagram results toward source mmA1 and source B is shown in Fig. 1, corresponding to Fig. 5 in the original paper. The warm and hot temperature components toward mmA1 are ≈560 K and ≈2600 K, respectively. The total column density, considering the contribution from both temperature components, is $N_{\mathrm{warm+hot}} \approx 1.39 \times 10^{21}$ cm^{-2}. Toward source B, we find a higher column density but a lower temperature.

The full temperature and column density maps are shown in Fig. 2 (Fig. 6 in the original paper), where the results for the cold component (left column) remain unchanged. With the corrected values, the H_2 column densities of the warm component are about two magnitudes lower compared to the cold component. The temperature of the warm component ranges between 250 K and 600 K. In the hot component, the column densities are about two orders of magnitude lower, of namely $N_{\mathrm{hot}} \approx 10^{19}$ cm^{-2}, compared to the warm component and the temperatures are 1000–2500 K.

The median temperature is 440 K and 1700 K for the warm and hot component, respectively, and the median column density is 8.7×10^{20} cm^{-2} and 5.8×10^{18} cm^{-2}, respectively. In absolute numbers, the median uncertainties are $\log \Delta N_{\mathrm{warm}} = 0.24 \log \mathrm{cm}^{-2}$, $\log \Delta N_{\mathrm{hot}} = 0.73 \log \mathrm{cm}^{-2}$, $\Delta T_{\mathrm{warm}} = 60$ K, and $\Delta T_{\mathrm{hot}} = 680$ K. Tables 1 (line-integrated intensities) and 2 (excitation diagram results) show corrected versions of Tables A.1 and A.2 of the original paper, respectively.

In Sect. 4.1 of the original paper, we compared the derived H_2 column densities of IRAS 23385 to the L1157 outflow (Nisini et al. 2010). With the corrected values, we find that the H_2 column densities of IRAS 23385 are not four, but two to three orders of magnitude higher. With JWST we are, for the first time, able to probe high-column density regions (>10^{21} cm^{-2}) thanks to the higher angular resolution.

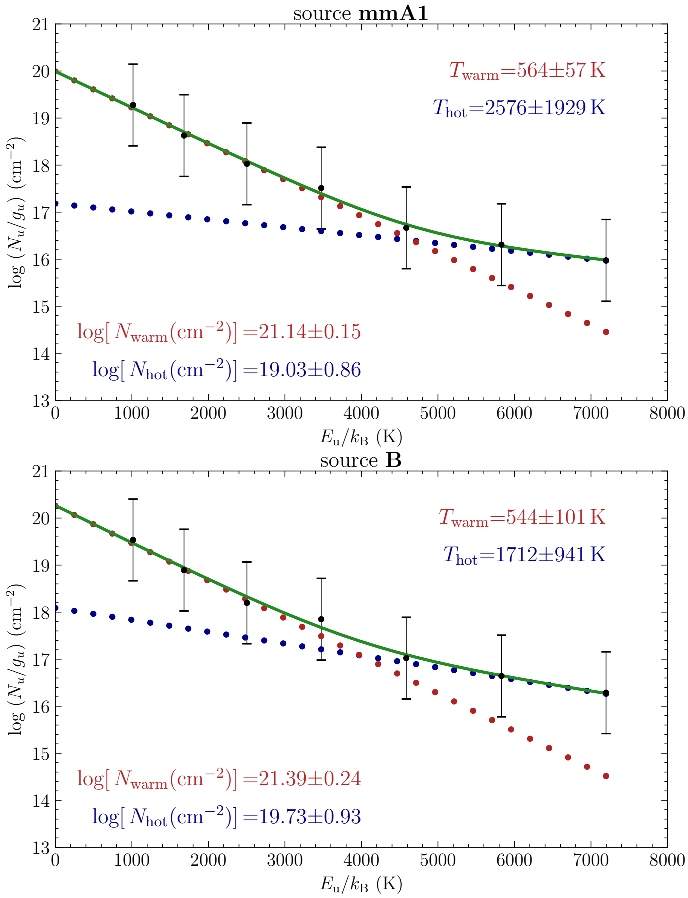

Fig. 1. Example of the H_2 excitation diagram analysis with `pdrtpy` of source mmA1 (top) and source B (bottom). The observed data are shown in black and the two-component fit is shown by red and blue dots, which correspond to the warm and hot component, respectively, and the total fit is indicated by a green line.

Table 1. Line-integrated intensities of H_2 (extinction-corrected, adopting values of A_K = 7, 5, and 3 mag) derived from a Gaussian fit to the observed line profiles (Sect. 3.3).

Position	Line-integrated intensity of H_2 0–0						
	S(1)	S(2)	S(3)	S(4)	S(5)	S(6)	S(7)
	(10^{-17} W m^{-2} arcsec^{-2})						
A_K = 7 mag							
mmA1	4.1	3.2	13.3	5.2	6.6	2.4	7.3
mmB	4.0	3.6	11.5	6.5	10.6	4.0	10.8
A/mmA2	6.2	4.8	20.6	8.6	12.0	4.1	11.8
B	7.5	5.9	19.6	11.2	15.0	5.2	14.9
S1	7.8	6.7	32.8	15.4	31.1	13.8	32.9
S2	3.0	2.2	4.1	2.5	3.2	1.3	3.4
S3	1.6	1.3	1.8	3.3	2.2	1.1	4.6
S4	3.5	2.8	8.1	3.2	4.8	2.3	5.9
A_K = 5 mag							
mmA1	1.6	1.3	3.5	2.2	2.9	1.0	3.1
mmB	1.6	1.5	3.0	2.7	4.7	1.6	4.5
A/mmA2	2.4	1.9	5.4	3.6	5.3	1.7	5.0
B	2.9	2.4	5.2	4.7	6.6	2.1	6.3
S1	3.1	2.7	8.7	6.5	13.7	5.6	13.9
S2	1.2	0.9	1.1	1.1	1.4	0.5	1.4
S3	0.6	0.5	0.5	1.4	1.0	0.5	1.9
S4	1.4	1.1	2.1	1.3	2.1	0.9	2.5
A_K = 3 mag							
mmA1	0.6	0.5	0.9	0.9	1.3	0.4	1.3
mmB	0.6	0.6	0.8	1.1	2.0	0.7	1.9
A/mmA2	1.0	0.8	1.4	1.5	2.3	0.7	2.1
B	1.1	0.9	1.4	2.0	2.9	0.9	2.7
S1	1.2	1.1	2.3	2.7	6.0	2.3	5.9
S2	0.5	0.4	0.3	0.4	0.6	0.2	0.6
S3	0.3	0.2	0.1	0.6	0.4	0.2	0.8
S4	0.5	0.4	0.6	0.6	0.9	0.4	1.1

Notes. Transition properties are listed in Table 1 in the original paper.

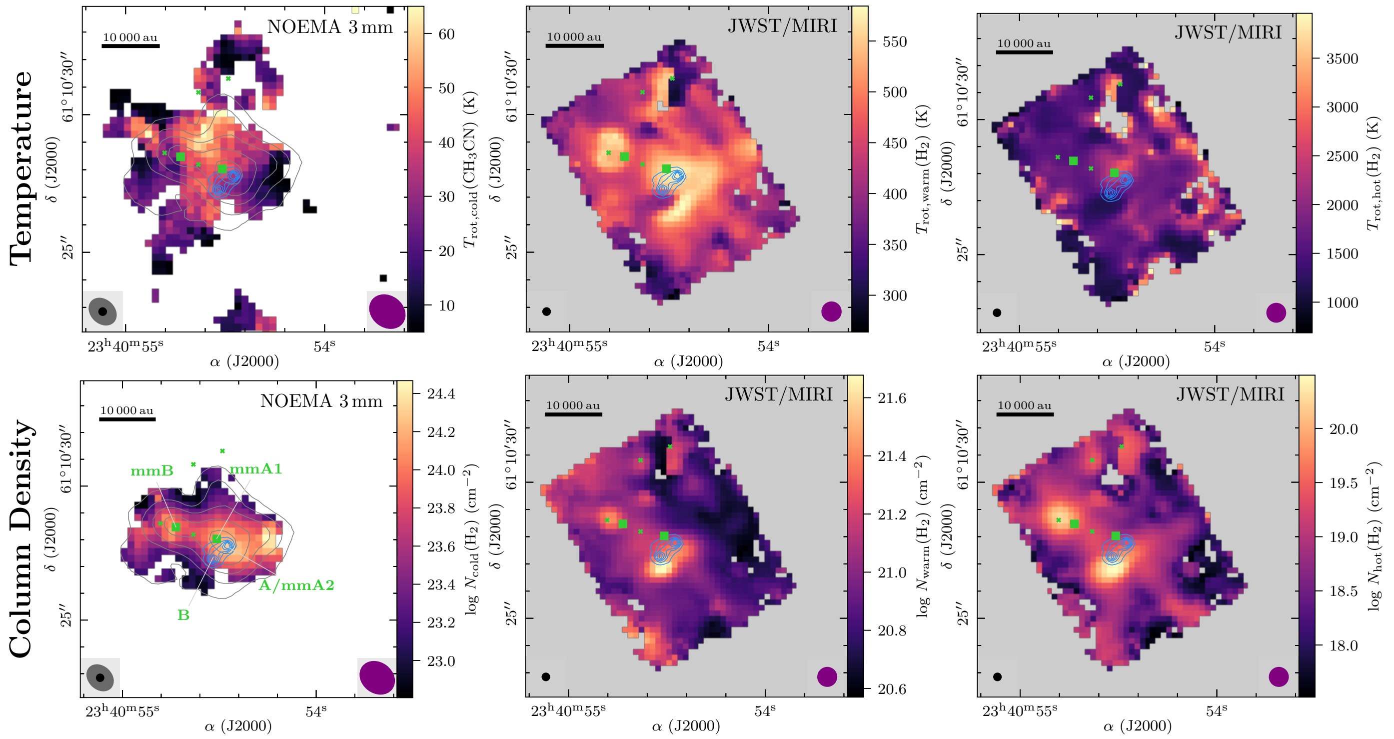

Fig. 2. Temperature and H_2 column density of the gas components in IRAS 23385 derived using CH_3CN and H_2 as a diagnostic tool (Sects. 3.3 and 3.4). In the top and bottom panels, the rotation temperature and H_2 column density maps, respectively, of the cold (left), warm (center), and hot (right) components are shown in color. The angular resolution of the line data is indicated by a purple ellipse in the bottom right corner. The JWST/MIRI 5.2 μm continuum is presented by blue contours with contour levels at 5, 10, 15, 20, and $25 \times \sigma_{\rm cont,5\,\mu m}$ and the angular resolution is highlighted by a black ellipse in the bottom left corner. The NOEMA 3 mm continuum (top and bottom left panels) is highlighted by gray contours with levels at 5, 10, 20, 40, and $80 \times \sigma_{\rm cont,3\,mm}$ and the synthesized beam is highlighted by a gray ellipse in the bottom left corner. All continuum sources are labeled in green in the bottom left panel and the millimeter continuum sources are marked by green squares. Several shock positions are indicated by green crosses (Sect. 3.2).

Table 2. Fit results from the H_2 excitation diagram analysis with `pdrtpy` (Sect. 3.3) with a warm and hot component, adopting values of A_K = 7, 5, and 3 mag.

Position	Warm component		Hot component	
	Temperature $T_{\rm warm}$ (K)	Column density $\log N_{\rm warm}$ (cm^{-2})	Temperature $T_{\rm hot}$ (K)	Column density $\log N_{\rm hot}$ (cm^{-2})
		A_K = 7 mag		
mmA1	564 ± 57	21.14 ± 0.15	2576 ± 1929	19.03 ± 0.86
mmB	505 ± 96	21.18 ± 0.24	1494 ± 455	19.79 ± 0.57
A/mmA2	572 ± 67	21.30 ± 0.16	2149 ± 1355	19.38 ± 0.87
B	544 ± 101	21.39 ± 0.24	1712 ± 941	19.73 ± 0.93
S1	531 ± 94	21.43 ± 0.20	1532 ± 361	20.26 ± 0.43
S2	408 ± 90	21.19 ± 0.36	1333 ± 401	19.47 ± 0.60
S3	548 ± 196	20.68 ± 0.54	3233 ± 8318	18.69 ± 2.29
S4	481 ± 57	21.16 ± 0.18	1791 ± 585	19.30 ± 0.51
		A_K = 5 mag		
mmA1	510 ± 103	20.76 ± 0.28	1628 ± 797	19.10 ± 0.85
mmB	369 ± 121	21.01 ± 0.50	1264 ± 263	19.69 ± 0.41
A/mmA2	439 ± 119	21.03 ± 0.37	1261 ± 326	19.72 ± 0.55
B	356 ± 132	21.29 ± 0.57	1175 ± 249	19.96 ± 0.45
S1	383 ± 100	21.23 ± 0.36	1336 ± 192	20.10 ± 0.27
S2	322 ± 102	21.03 ± 0.58	1214 ± 300	19.26 ± 0.50
S3	295 ± 186	20.88 ± 1.21	1380 ± 615	19.08 ± 0.76
S4	393 ± 82	20.90 ± 0.34	1396 ± 335	19.26 ± 0.44
		A_K = 3 mag		
mmA1	346 ± 126	20.67 ± 0.60	1205 ± 280	19.21 ± 0.47
mmB	324 ± 140	20.75 ± 0.74	1313 ± 337	19.26 ± 0.47
A/mmA2	331 ± 128	20.88 ± 0.64	1186 ± 246	19.47 ± 0.42
B	312 ± 142	21.04 ± 0.80	1218 ± 298	19.52 ± 0.48
S1	334 ± 124	20.97 ± 0.59	1395 ± 272	19.66 ± 0.33
S2	289 ± 113	20.77 ± 0.79	1263 ± 369	18.82 ± 0.55
S3	275 ± 185	20.58 ± 1.38	1490 ± 776	18.60 ± 0.82
S4	327 ± 96	20.69 ± 0.54	1352 ± 333	18.94 ± 0.44

References

Gieser, C., Beuther, H., van Dishoeck, E. F., et al. 2023, A&A, 679, A108
Nisini, B., Giannini, T., Neufeld, D. A., et al. 2010, ApJ, 724, 69